https://doi.org/10.5194/essd-2026-558
Preprint. Discussion started: 23 July 2026

Earth System Science Data Discussions

Sea Surface Temperature Upwelling Index for West Iberia (1982-2021)

Joaquim Dias[1,2], Gregory P. King[1], Paola Castellanos[1,3]

[1]Marine and Environmental Sciences Centre (MARE), Aquatic Research Network (ARNET), Faculdade de Ciências, Universidade de Lisboa, Campo Grande, 1749-016 Lisboa, Portugal
[2]Departamento de Ciências da Terra e Energia (DCTE), Faculdade de Ciências, Universidade de Lisboa, Campo Grande, 1749-016 Lisboa, Portugal
[3]Portuguese Institute for Sea and Atmosphere, 1495-165 Lisboa, Portugal

Correspondence to: Paola Castellanos (paola.ossa@ipma.pt)

Abstract. Cloud cover introduces extensive gaps in sea-surface temperature (SST) fields derived from infrared satellite measurements, and gap frequency rises further when differencing data to compute an SST-based upwelling index. Averaging can eliminate gaps but degrades spatio-temporal resolution, whereas interpolation preserves resolution but requires robust methodology. The CoRTAD database — a 21-year global ocean satellite SST dataset, gap-free, at 4 km resolution and weekly averaged — in which missing observations were mitigated by merging night- and day-passes from the Pathfinder V5.3 satellite record and computing weekly means. Residual SST gaps were filled first with a 3 × 3-pixel spatial median and, where necessary, with a piecewise cubic Hermite interpolating polynomial. The resulting spatial and temporal resolution supports observation of sub-mesoscale to mesoscale coastal-ocean processes. From CoRTAD, SSTs at near- and offshore locations for West Iberia (37°–44° N) were extracted and a coastal upwelling index (UI^{sst}) calculated for the period January 1982 to December 2021. The nearshore (midshelf) climatology derived from this dataset successfully identifies established recurrent upwelling centres along the West Iberian coast, which were previously detectable only in cloud-free synoptic SST imagery, thereby supporting the validity of the dataset. Monthly climatology reveals no north-south differences in upwelling intensity or season end-date, but shows that the central region between Cabo Carvoeiro (~39° N) and the River Douro (~41° N) has a notably later upwelling season onset (July/August versus June/July). With continuous satellite scatterometer winds available since 1999, the stage is set to compare an Ekman-derived upwelling index with the SST-derived index. This study demonstrates that a high-resolution, gap-free satellite

https://doi.org/10.5194/essd-2026-558
Preprint. Discussion started: 23 July 2026

Open Access Earth System Science Data Discussions

SST dataset combined with targeted interpolation enables robust characterisation of coastal upwelling dynamics over multi-decadal timescales.

1 Introduction

Coastal upwelling occurs to preserve continuity, in response to offshore Ekman transport of the ocean upper layer generated by surface wind stress along the coast. Once the effects of the upper layer offshore transport overcome the effects of water column stratification near the coast, colder and comparatively high in nutrients lower layer water, it is draw up into the photic surface layer, stimulating biological productivity and creating good fishing regions. Regions with upwelling ecosystems only constitute about 0.2% of the ocean surface but account for roughly 20% of the world's fish harvest (Pauly and Christensen, 1995; FAO, 2022). Stimulated by concerns of fish stock levels and the impacts of global climate change on the coastal ecosystem, there is increased need to monitor coastal upwelling and quantify its strength and variability in space and time.

Traditionally, two types of indices have been developed to monitor the strength of upwelling: one based on wind forcing (Ekman index), and one based on the sea surface temperature (SST) gradient (SST upwelling index). The Ekman index estimates the offshore Ekman transport based on geostrophic winds calculated from measurements of surface atmospheric pressure fields (Bakun, 1973), or (more recently) on satellite measured winds (Alvarez et al., 2008). The SST upwelling index is an estimate of the temperature gradient across the thermal front separating cold upwelled coastal water from warmer offshore water. The Ekman and SST upwelling indices should be correlated, but the correlation is not simple nor is it guaranteed to always exist, since other mesoscale and regional scale oceanic processes, than upwelling, may act to modify the differences in temperature between the coastal and offshore waters. Furthermore, the coastal upwelling intensity is regulated by the interplay of wind stress and water column stratification what could lead to a breakdown in the correlation between Ekman and SST indices (Siemer et al., 2021).

The Ekman index was developed by the NOAA Pacific Fisheries Environmental Laboratory (PFEL) and is widely used. The SST upwelling index, on the other hand, has received much less attention. However, due to the global coverage and accessibility of online databases of high-resolution satellite measured SST, there is growing interest in using the SST upwelling index (Leitão et al., 2019; Benazzouz et al., 2014; Santos et al.,

https://doi.org/10.5194/essd-2026-558
Preprint. Discussion started: 23 July 2026

2005; Demarcq and Faure, 2000; Demarcq, 1998; Nykjær and Van Camp, 1994). Furthermore, since the full biological response to upwelling depends on the delivery of nutrients into the photic layer close to the sea surface, brought by the colder lower layer upwelled water, the SST index is potentially a more sensitive indicator of the biological response than the Ekman index.

For practical reasons, the SST gradient across the thermal front created by coastal upwelling is estimated as the difference in SST between a station located near the coast and a station located offshore in the adjacent open ocean. The near-coast and offshore locations vary according to local oceanographic and geographic characteristics of the study area. The near-coast location is usually taken to be over the continental shelf between the shelf break (typically the 200-m isobath) and approximately the 30-m isobath (hereinafter referred to as the midshelf). This suggests that an SST upwelling index (UI^{sst}) for an almost North-South orientation of the coast, such as occurs for the West Iberian Peninsula, can be defined as

$$\mathbf{UI^{SST}}(\varphi, t) = \mathbf{T^{mid}}(\varphi, t) - \mathbf{T^{off}}(\varphi, t) \,, \qquad (1)$$

where $\mathbf{T^{mid}}$ is the midshelf SST, $\mathbf{T^{off}}$ is the offshore SST, and φ and t are the corresponding latitude and time.

An appropriate offshore location varies from region to region and must be determined through investigation, but should be far enough away that the offshore SST is not disturbed by upwelling filaments --- in the case of west Iberia, filaments have been found to extend as far as 200-250 km from the coast (Fiúza, 1983).

Although UI^{sst} looks simple to calculate, it is not straightforward. Satellite SST measurements have many sources of noise but the main contribution comes from gaps in the observations, primarily due to clouds but also from instrument failure. The differencing operation necessary to calculate the SST upwelling index creates more gaps in UI^{sst} than contained in T^{mid} or T^{off}. In order to minimize the effect of gaps, SST data are averaged over space and time. As a result, UI^{sst} is generally reported as a monthly average at spatial resolutions of several tens of kilometers (Nykjær and Van Camp, 1994; Santos et al., 2005). However, higher space and time resolution is needed in order to identify localized regions of upwelling and to correlate upwelling with the timing of natural events that affect the functioning of marine ecosystems (Bograd et al., 2009).

https://doi.org/10.5194/essd-2026-558
Preprint. Discussion started: 23 July 2026

The primary objective of this study is to use satellite-derived SST data to calculate an upwelling index for the west Iberian coast, with spatial and temporal resolutions in the transition domain from submesoscale to mesoscale, where the dynamical effects of Earth's rotation begin to dominate. For this purpose, we use Version 6 of the Coral Reef Temperature Anomaly Database (CoRTAD), which provides a global, 4-km resolution, weekly averaged SST product developed from Pathfinder V5.3 data, spanning the period 1982–2021 (Saha et al., 2018a, 2018b). This dataset is produced by the National Oceanic and Atmospheric Administration's (NOAA) National Centers for Environmental Information (NCEI). This article describes the SST upwelling index data for 1982–2021, available as a historical Earth Observation product for the Portuguese coastal region via the CoastNet Infrastructure platform (https://coastnet.pt/). Future work will extend this analysis to the present, enabling the provision of a near–real-time SST upwelling index of west Iberian on the CoastNet geoportal.

The remainder of the paper is structured as follows. Section 2 gives a brief overview of the West Iberia upwelling system, and the present state of knowledge of its interannual and long-term variability. The data and our methodology are described in Section 3. The SST time series and a study of the climatology and interannual variability of T^{mid}, T^{off}, and UI^{sst} is presented in Section 4. In Section 5 we present our conclusions and suggestions for future directions.

2 Seasonal upwelling and its interannual variability along West Iberia

The general bathymetry of the western Iberian continental margin is shown in Fig. 1. The principal geographical features off the west coast that may play an influential role on the spatial distribution and variability of the upwelling front are indicated in the figure. The continental margin includes the western coasts of Portugal and Spain. South of about 39º N the continental margin is characterized by a narrow shelf (~25 km) and a not very steep continental slope (~0.03), while to the north the shelf is wider (50 – 60 km) and the continental slope is steeper (~0.06). Several canyons cut the West Iberian continental slope, the most prominent of which is Nazaré Canyon (39.4º N), just north of Cape Carvoeiro (CC). Most of the river runoff occurs to the north of Lisbon (38.7º N) where several rivers deliver fresh water to the shelf. The Tagus (38.7º N), Douro (41.1º N) and Minho (41.9º N) are the most significant, but the Rías (in the northwest of Spain) make an important contribution as well (Peliz et al., 2005, 2002).

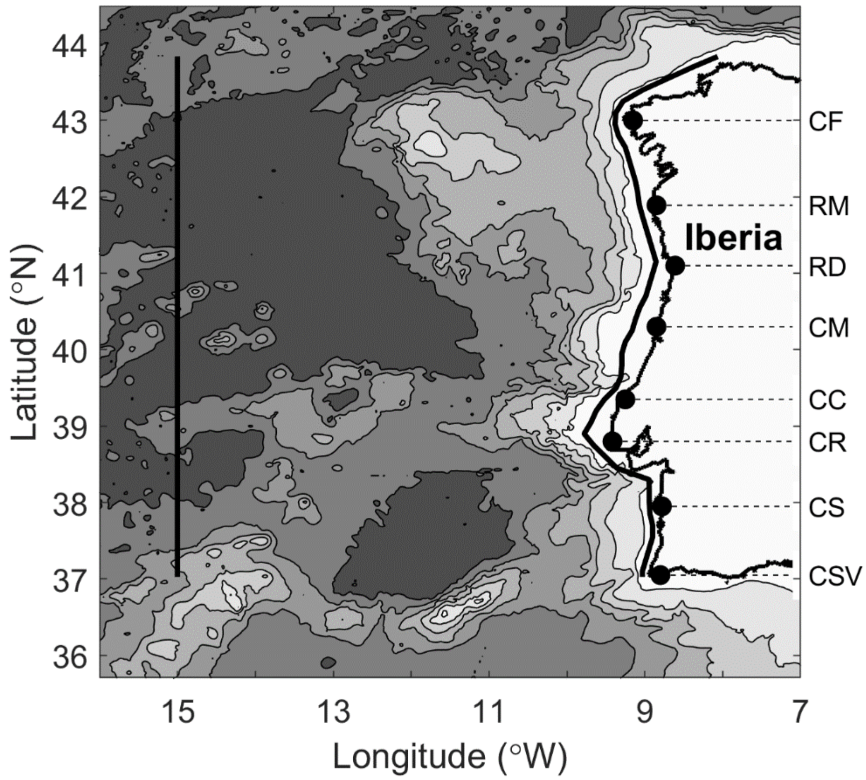

Figure 1: General bathymetry of the Western Iberian continental margin (bathymetry data downloaded from http://topex.ucsd.edu/marine_topo/; Smith and Sandwell (1997)). The isobaths correspond to 0.2, 1, 2, 3 and 5 km. The midshelf line (the bold line between the 200-m isobath and the coast) and the offshore line (bold line at 15º W) used to define an upwelling index are shown. Geographical features marked by their latitude on the figure are: CF: Cape Finisterre, RM: River Minho, RD: River Douro, CM: Cape Mondego, CC: Cape Carvoeiro, CR: Cape Roca, CS: Cape Sines, CSV: Cape São Vicente.

The mainly seasonal character of upwelling along West Iberia is described in review papers by Barton (1998), Aristegui et al. (2006), Relvas et al. (2007), Ambar and Dias (2008), Arístegui et al. (2009). Persistent winds from the north along West Iberia generate coastal divergence, which then induces coastal upwelling. The coastal divergence generates a pressure gradient that drives a geostrophic southward flow in the surface layer (Portuguese Coastal Current) (e.g., Peliz and Fiuza, 1999). The current is disturbed by mesoscale eddies, jets, and filaments that transport upwelled water to the open ocean. The persistent northerly winds start in March and continue into September, with summer months, July through September, being the period of strongest upwelling conditions. There is a lag of one to two months between the average regime of northerly favourable winds and the

https://doi.org/10.5194/essd-2026-558
Preprint. Discussion started: 23 July 2026

Open Access Earth System Science Data Discussions

coastal upwelling signal, as detected by SST anomalies (Fiúza et al., 1982; Nykjær and Van Camp, 1994). In autumn the wind regime reverses. The resulting coastal convergence and ocean meridional density gradient drive a poleward surface current that transports warm and salty water northward along the shelf (Portuguese Coastal Counter Current) (Frouin et al., 1990; Haynes and Barton, 1990). Studies by Fiúza et al. (1982), Haynes et al. (1993), Santos et al. (2004) show that winter upwelling episodes are sporadic, have a shorter duration, and are less intense than in summer.

The interannual and long-term variability of the Iberian upwelling system has been addressed in recent papers by Lemos and Pires (2004), Santos et al. (2005), Lemos and Sansó (2006), Arístegui et al. (2006), Sánchez et al. (2007), Álvarez-Salgado et al. (2008), Alvarez et al. (2008), Leitão et al. (2019), Bustos et al. (2024). Arístegui et al. (2006) analysed SST data (COADS database) collected by merchant ships along the Eastern North Atlantic coast from 10º N to 43º N for the period 1950 to 1995. They found evidence of an intensive cooling affecting the whole region and all seasons throughout the 1970s. They also investigated possible links between the SST anomaly field and climate fluctuations associated with the North Atlantic Oscillation (NAO) and the Pacific El Niño/Southern-Oscillation (ENSO). A negative SST-NAO correlation (ranging from -0.19 to -0.25) for the Iberian coast were found when only upwelling favourable months were considered, suggesting that negative SST anomalies (stronger upwelling) might be related to positive NAO anomalies.

Santos et al. (2005) used high-resolution satellite-derived SST to study the variability of the Canary Upwelling Ecosystem (12º to 43º N) for the period 1982 to 2001. They found that the SST anomaly field in the open ocean had a quasi-regular decadal oscillation. However, they interpreted the variability in the Iberian and Northwest Africa (from 22º to 30º N) coastal areas as a shift in upwelling intensity - from weaker upwelling (from 1982 to 1992–93) to stronger upwelling (from 1992–93 to 2001). This shift in upwelling intensity and its timing was attributed to the long-term variability of the northerly winds along the West Iberian coast.

Leitão et al. (2019) estimated a monthly SST upwelling index along the Portuguese coast for the period from 1950 to 2010. They used remote sensing SST data from the 4-km Pathfinder version 5 collection (1985–2009) and in situ SST data from ICOADS (1950–2010). They report for the West Iberia coast a decrease of the SST upwelling index in the period from 1956 to late 1970s, followed by a non-significant intensification in a more recent period, from 1985 to 2009. Their global results showed that sudden, wide amplitude

https://doi.org/10.5194/essd-2026-558
Preprint. Discussion started: 23 July 2026

shifts frequently occur at a decadal time-scale with consecutive intensification or weakening (cascading patterns) that can last for a few decades. The decadal-scale SST oscillation reported by Santos et al. (2005) and Leitão et al. (2019) is explained by some authors as the result of a coupled atmosphere-ocean interaction in the Atlantic basin (Marshall et al., 2001; Kravtsov et al., 2008).

The long-term atmosphere-ocean coupling off the West Iberian coast was explored by Sánchez et al. (2007) using Canonical Correlation Analysis of SST and ocean winds. Using an 18-year regional-scale data set covering the period 1981 to 1997 with a space resolution of 1º×1º and time resolution of 1-month, the authors found coupled SST-wind upwelling/downwelling patterns clearly related with the NAO signal, with much of the variability concentrated at quasi-biennial frequencies.

Alvarez et al. (2008) analyzed the spatial and temporal variability of upwelling regime along the western coast of the Iberian Peninsula using Ekman index data from the PFEL database for the period 1967 to 2006. The monthly upwelling trends during this period indicate a weakening in upwelling intensity during most of the year, with the exception of February, June and July.

Lemos and Pires (2004) analysed winds measured at four coastal stations along the west Iberian coast for the period 1941-2000, and Lemos and Sansó (2006) analysed ocean temperature data for the 20th century (World Ocean Database 2001). These authors found a weakening of northerly upwelling-favourable winds from the 1940s onward, and a fading in the shelf-ocean temperature gradients. Their results suggest a long-term weakening of the costal upwelling regime along West Iberia.

More recently, Bustos et al. (2024) applied machine learning techniques to analyse long-term variability in the four major Eastern Boundary Upwelling Systems (EBUS) worldwide over the period 1993–2019. They used oceanographic and atmospheric data from observations, models, and reanalysis products. Long-term changes in dominant spatial patterns were assessed by comparing 2007–2019 with the reference period 1993–2006. For the west Iberian Peninsula region, their results show an increase in upwelling-favourable winds and a reduction in nearshore SST. These changes, indicative of increased upwelling intensity, are attributed to a poleward shift of the North Atlantic Subtropical High, consistent with Hadley cell expansion under a warming climate.

From this brief overview, it is evident that there is some disagreement among authors regarding the interannual and long-term variability of the Iberian upwelling system. These

https://doi.org/10.5194/essd-2026-558
Preprint. Discussion started: 23 July 2026

discrepancies may result from differences in datasets and temporal coverage and warrant further investigation.

3 Data and Methods

3.1 CoRTAD SST data

The West Iberia SST upwelling index presented in this work, was computed using the Version 6 of the Coral Reef Temperature Anomaly Database (CoRTAD), a global, 4-km, resolution, SST and related thermal stress metrics dataset (Saha et al., 2018a). The CoRTAD contains weekly averaged SSTs, and other derived SST products relevant for coral reef studies. This dataset is based on the Pathfinder V5.3 (PFV53) L3C SST dataset (Saha et al., 2018b) and is created with support from the NOAA Coral Reef Conservation Program. The database was accessed on 18 June 2022 to retrieve a subset of the global, gap-free, weekly averaged SST dataset covering the area shown in Fig. 1 for the period from 2 January 1982 to 31 December 2021.

CoRTAD datasets were originally developed by Selig et al. (2010) using data from the Pathfinder Version 5.0 collection, in order to quantify the spatial, 10 km or less, and temporal characteristics of temperature anomalies related to both coral bleaching and disease. They created a 4-km resolution, 21-year global ocean weekly-averaged SST database, using daytime and nighttime Pathfinder data with a quality flag of 4 or better. If only day or night data were available, they used those data. With this approach, the number of missing pixels was reduced by 25% without significant change in the accuracy. The overall mean difference in the accuracy relative to in situ data of the nighttime-only average and CoRTAD average, was less than 0.05 °C.
Pathfinder data with a quality flag ≥4 indicate that SST pixel estimates passed the "reference" quality test (Kilpatrick et al., 2001). This test requires the absolute difference between the estimated SST and a reference SST from the Reynolds Optimum Interpolation Sea Surface Temperature (OISST) dataset—a long-term, satellite- and in situ–based product (Reynolds et al., 2002)—to be ≤2 °C. During the construction of CoRTAD, Selig et al. (2010) modified this criterion to preserve warming anomalies by including observations in which weekly SST values were up to 5 °C warmer than OISST, while retaining the −2 °C threshold for negative differences. This adjustment reduced missing data to 21.2% of the dataset.

https://doi.org/10.5194/essd-2026-558
Preprint. Discussion started: 23 July 2026

Selig et al. (2010) generated a near gap-free dataset by applying a 3x3 median spatial filter, in which missing pixel values were replaced with the median of adjacent pixels. Remaining gaps were subsequently filled using temporal interpolation based on a piecewise cubic Hermite interpolating polynomial. The authors found that temperature data in the CoRTAD were accurate when compared with in situ loggers over a wide range of coral locations and depths, with a mean difference of 0.11 °C, which was within the range of the typical accuracy of the in-situ temperature loggers themselves (+/- 0.2 °C).

3.2 Near-coast and offshore locations

In order to calculate the SST upwelling index $\mathbf{UI^{SST}}$ (Eq. (1)), appropriate locations near the coast and offshore must be identified. Ideally the near-coast locations should be shoreward of the thermal front that separates upwelled waters from offshore waters, but not so close to shore that inner shelf dynamics contaminate the measurement. For example, very close to the shore the shallow depths result in the overlap of surface and bottom boundary layers, which for an along-shore wind results in a decrease of the cross-shelf Ekman transport. Furthermore, Peliz et al. (2002) and Relvas et al. (2007) report that during the upwelling season inner-shelf counter-flows can occur that advect warm water poleward, creating a thermal front shoreward of the upwelled water. For pragmatic reasons, we followed Nykjær and Van Camp (1994) and identified the near-coast locations using the midshelf line - a line (see Fig. 1) located approximately halfway between the outer edge of the continental shelf (the 200-m isobath) and the coast, between latitudes 37.0° N and 43.8° N. The choice of the midshelf line to represent the near coast upwelling affected region, is supported by the work of Fiúza (1983) who used remotely sensed SST and coastal wind measurements to characterize Portuguese coastal upwelling patterns off the west and south coasts. He found that along the west coast the upwelling offshore thermal front pulses onshore-offshore in response to the intensity of northerly winds, and ranged in position from 30 to 200 km from the coast. Further support for choosing the midshelf line comes from a study by Relvas et al. (2007), who computed a frontal probability map for west and south Iberia using summer SST images from the years 2001-2005. Their frontal probability map shows thermal frontal structures aligned with the coast and with a tendency to be located offshore of the midshelf line.

To determine appropriate offshore locations, we examined meridional profiles of monthly mean SST for the period 1982–2021 at longitudes between 10° and 22° W. During the summer months, these profiles reveal a clear cooling signature associated with coastal

https://doi.org/10.5194/essd-2026-558
Preprint. Discussion started: 23 July 2026

upwelling at 10° W (approximately 100 km from the coast), which is no longer evident west of ~12° W (approximately 300 km offshore). Between 12º and 17º W, the meridional profiles exhibit an approximately linear decrease in SST with increasing latitude. Farther west (≳18° W), the latitudinal SST variation becomes distinctly non-linear, indicating a transition to an oceanic region characterized by more complex dynamics. On this basis, we selected 15º W as our offshore line (approximately 550 km from the coast), with the same latitude limits as the midshelf line. The midshelf and offshore lines are shown in Fig. 1.

3.3 Data organization and averaging

Temperatures along the midshelf and offshore lines, from the southern to the northern limits of West Iberia (37.0°-43.8° N), were extracted from the weekly CoRTAD version 6 SST maps and organized into three-dimensional matrices, $\mathbf{T}^{\mathbf{off}}$ (offshore SST) and $\mathbf{T}^{\mathbf{mid}}$ (midshelf SST). Rows are indexed by latitude, columns by week, and the 3rd dimension by year, resulting in two matrices of a size 165x52 x40 each. At a given time, the SST distribution as a function of latitude will be referred to as an SST profile.

The annual cycle is defined as the expected evolution of a climatic variable through the year. It is calculated as a weekly, monthly and 3-month climatology. The annual cycle based on a weekly climatology is calculated as the average of all week-1 profiles, all week-2 profiles, etc., based on a monthly climatology by averaging all January profiles, all February profiles etc., and based on a 3-month climatology by averaging all profiles in a season. Seasons are 13 weeks long and denoted by JFM (January, February, March), AMJ (April, May, June), JAS (July, August, September), and OND (October, November, December), which are also referred to, respectively, as 'winter', 'spring', 'summer', and 'autumn'.

4. Results and Discussion

4.1 Full space-time resolution

Table 1 summarizes statistical metrics for the SST matrices, $\mathbf{T}^{\mathbf{off}}$ and $\mathbf{T}^{\mathbf{mid}}$, and for the upwelling index matrix $\mathbf{UI}^{\mathbf{SST}}$. A total of 165 SST records are missing across all matrices, corresponding to the SST profiles for the midshelf and offshore lines during the final week of the dataset (25–31 December 2021). Because this period corresponds to the end of the dataset, the temporal interpolation scheme described by Selig et al. (2010) could not be applied to fill these gaps. In addition to these 165 missing values, the $\mathbf{T}^{\mathbf{mid}}$ matrix, and

https://doi.org/10.5194/essd-2026-558
Preprint. Discussion started: 23 July 2026

Open Access Earth System Science Data Discussions

consequently the $\mathbf{UI^{SST}}$ matrix, contains one additional gap resulting from the removal of a spurious temperature value (29.79 °C) recorded at the pixel located at 39.6° N during the week of 2–8 July 1983. Missing SST values were replaced with NaNs.

Table 1. Statistical metrics for the SST matrices $\mathbf{T^{off}}$ and $\mathbf{T^{mid}}$ and for the upwelling index matrix $\mathbf{UI^{SST}}$.

	Maximum ^{0}C)	Minimum (^{0}C)	Mean (^{0}C)	Standard deviation (^{0}C)	Median (^{0}C)	Skewness	No. of NaNs
$\mathbf{T^{off}}$	24.87	9.14	16.93	2.76	16.53	0.20	165
$\mathbf{T^{mid}}$	25.55	9.26	15.79	2.04	15.65	0.24	166
$\mathbf{UI^{SST}}$	10.95	-8.61	-1.14	1.59	-0.91	-0.42	166

To complement the statistical description, histograms of the data matrices were computed using 1 °C bins over the ranges 8–32 °C for the $\mathbf{T^{off}}$ and $\mathbf{T^{mid}}$ matrices and −10–15 °C for the $\mathbf{UI^{SST}}$ matrix (Fig. 2). The distributions are approximately symmetric, with absolute skewness values below 0.5 (Table 1). The $\mathbf{T^{off}}$ data exhibit a bimodal distribution consistent with the seasonality of SST. The primary peak, centered at 15.5 °C with approximately 4.8×10^4 counts, corresponds to winter conditions characterized by a deep surface mixed layer that stabilizes SST. The secondary peak, centered at 20.5 °C with approximately 3.4×10^4 counts, represents summer conditions, when a shallower mixed layer results in greater SST variability. This bimodal structure is not observed in the $\mathbf{T^{mid}}$ distribution because seasonal upwelling reduces SST contrasts between summer and winter near the coast.

https://doi.org/10.5194/essd-2026-558
Preprint. Discussion started: 23 July 2026

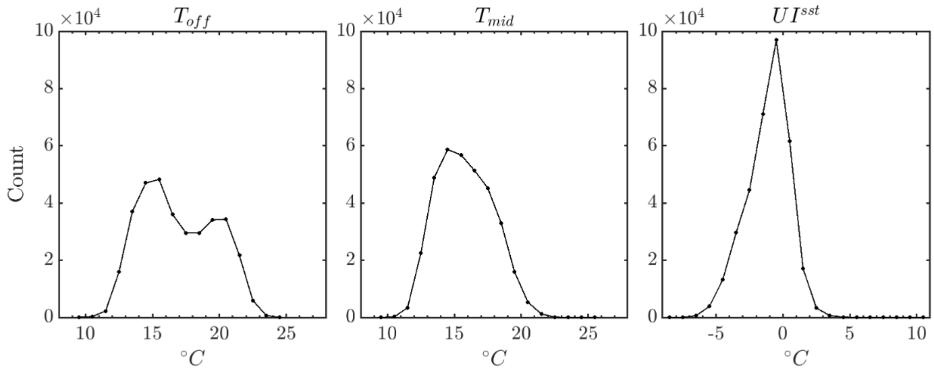

Figure 2. Histograms for $\mathbf{T^{off}}$, $\mathbf{T^{mid}}$ and $\mathbf{UI^{SST}}$ (left, middle and right panels, respectively), computed using 1 °C bins.

The SST and $\mathbf{UI^{SST}}$ profiles at the full space and time resolution of the CoRTAD dataset is shown in Fig. 3 and 4. The offshore SST (top panels) shows a space-time oscillation with a slow year-to-year variation. In contrast the midshelf SST (middle panels) has a complex appearance with significant year-to-year variability. The complexity of the midshelf SST is mainly caused by coastal upwelling occurring preferentially during the summer months There are well-defined cold features in the midshelf summer profiles: sharp SST minima occurring in the vicinity of Cape Carvoeiro at 39.4° N and Cape Roca at 38.8° N (labeled CC and CR in Fig. 1) and two broad cold features further north near the latitudes of the River Minho at 41.9° N and Cape Finisterre at 43.0° N (labeled RM and CF in Fig. 1).The upwelling index (bottom panels) inherits the complexity of the midshelf SST, and also emphasizes the onset, the end, and the intensity of the upwelling season, as well as its interannual variability.

https://doi.org/10.5194/essd-2026-558
Preprint. Discussion started: 23 July 2026

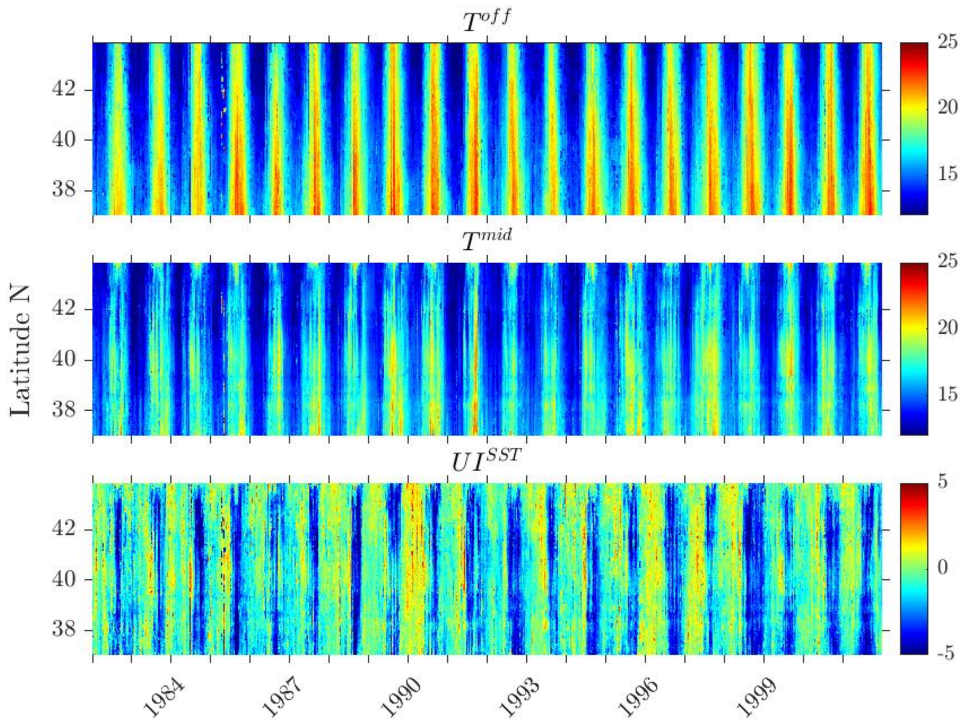

Figure 3. Time series of the CoRTAD SST and UI^{SST} (ºC) profiles: (top panel) $\boldsymbol{T}^{off}$, the offshore SST along 15º W; (middle panel) $\boldsymbol{T}^{mid}$, the midshelf SST; and (bottom panel) $UI^{sst} = \boldsymbol{T}^{mid}$ - $\boldsymbol{T}^{off}$, the upwelling index. The time series extends from the beginning of January 1982 through the end of December 2001.

https://doi.org/10.5194/essd-2026-558
Preprint. Discussion started: 23 July 2026

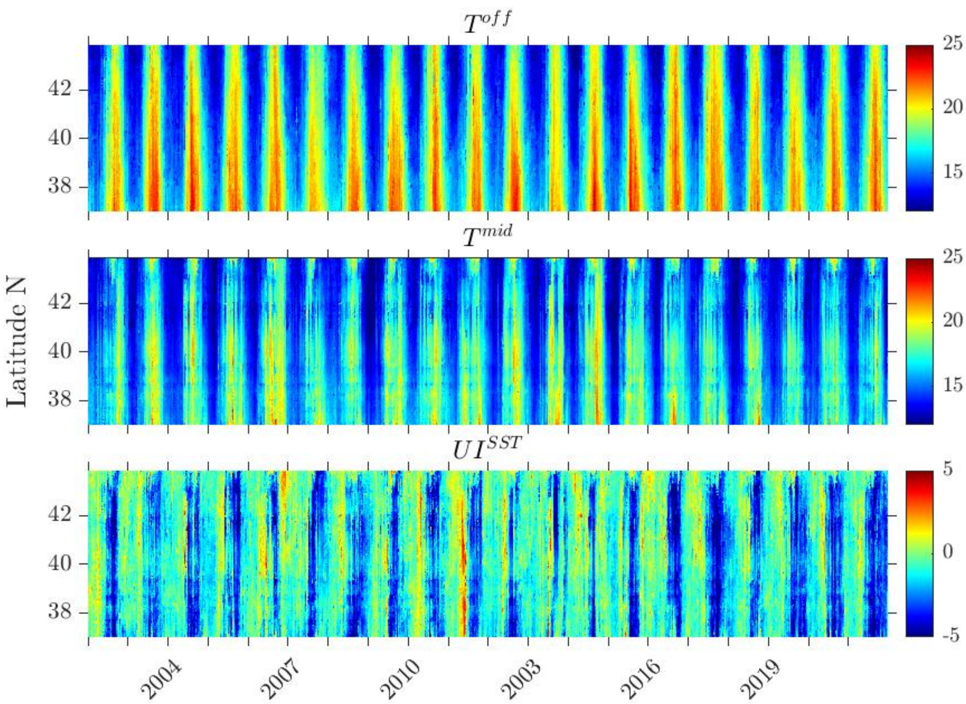

Figure 4. Time series of the CoRTAD SST and UI^{SST} (ºC) profiles: (top panel) $\boldsymbol{T^{off}}$, the offshore SST along 15º W; (middle panel) $\boldsymbol{T^{mid}}$, the midshelf SST; and (bottom panel) $UI^{sst} = \boldsymbol{T^{mid}}$ - $\boldsymbol{T^{off}}$, the upwelling index. The time series extends from the beginning of January 2002 through the end of December 2021.

4.2 The Annual Cycle

4.2.1 Weekly climatology

Annual cycles based on a weekly climatology are shown in Fig. 5. The offshore annual cycle (Fig. 5a) shows the SST increasing uniformly towards the equator, typical of the Northern Hemisphere at mid-latitudes, with a minimum near the end of March (~13ºC) and a maximum near mid to late September (~22ºC). The midshelf annual cycle (Fig. 5b) illustrates the effect of coastal upwelling: a non-uniform temperature decreases relative to the offshore SST profile, centered during the summer months (JAS). Pronounced cooling occurs near specific geographical locations, particularly around capes.

https://doi.org/10.5194/essd-2026-558
Preprint. Discussion started: 23 July 2026

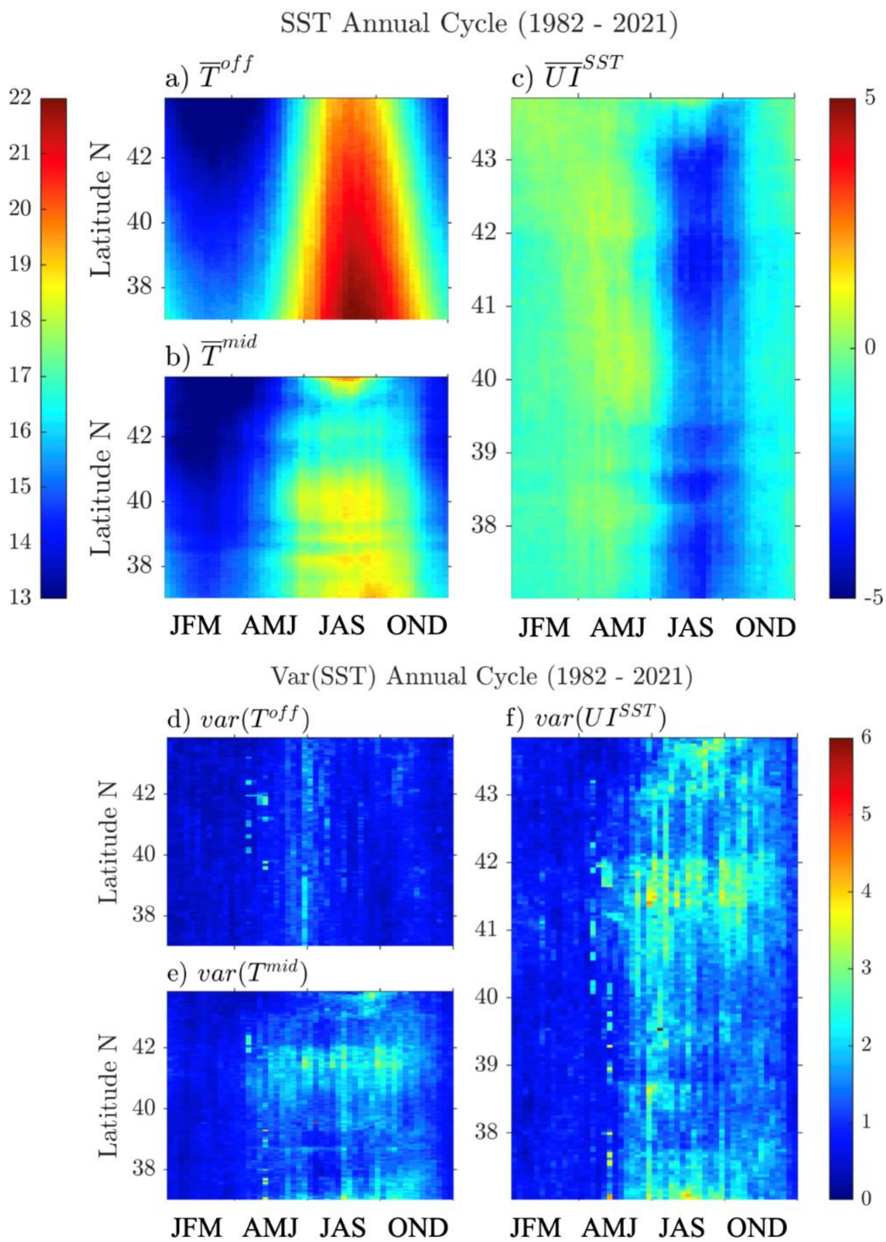

375 Figure 5. Weekly SST (ºC) climatology calculated using the CoRTAD version 6 filled dataset. From top to bottom: the annual cycle (a) $\overline{T}^{off}$; (b) $\overline{T}^{mid}$, and (c) $\overline{UI}^{SST}$; variance (ºC^2) relative to annual cycle (d) var(T^{off}) ; (e) var(T^{mid}) , and (f) var(UI^{SST}).

https://doi.org/10.5194/essd-2026-558
Preprint. Discussion started: 23 July 2026

The annual cycle of the upwelling index clearly identifies the upwelling season along the whole coast (dark blue in Fig. 5c). The figure shows a well-marked beginning of the upwelling season, occurring around June/July with lags of 2 to 4 weeks between different latitude bands. On the other hand, the end of the upwelling season is not so abrupt, extending through the autumn months (OND), but still maintaining the lag observed between latitude bands. The latitude bands for which the beginning of the upwelling season occurs earlier are also those where it ends later. From February to late June early July, a weak positive index ($\overline{UI}^{SST} \approx 1^{o}C$) is observed (more prominent north of 39.5ºN), and which is believed to correspond to the warm signature of the Portuguese Coastal Counter Current.

The variances of the SST and UI^{SST} time series relative to their respective weekly climatologies (Figures 5d–f) clearly reveal the variability associated with summer coastal upwelling. Bands of elevated $\mathrm{var}(UI^{SST})$ align with the latitudinal regions of stronger $\overline{UI}^{SST}$ (Figure 5c), as well as with the southern and northern limits of the western Iberian Peninsula, where the predominantly meridional orientation of the coastline is disrupted.

Furthermore, variability linked to the timing of the onset and termination of the upwelling season is evident, with elevated $\mathrm{var}(UI^{SST})$ values extending into the spring (AMJ) and autumn (OND) periods.

4.2.2 Three-month climatology

The annual cycle based on a 3-month climatology of the offshore and midshelf SST is shown in Fig. 6. The offshore profiles vary linearly with latitude (Fig. 6, left panel), and the meridional gradients for winter (JFM), spring (AMJ) and autumn (OND) are almost identical. The gradient in summer is smaller due to the transport of warmer water from the western basin of the North Atlantic by the dominant eastward zonal flow in the region, which occurs in response to the summer northward shift of the North Atlantic subtropical gyre and associated subtropical front. Another factor, that also contributes to the decrease of the meridional temperature gradient in summer, it is the seasonal meridional migration of Earth's net flux radiation positive areas, with its maximum shifted to the northern hemisphere at June solstice. Between autumn and spring, the midshelf profiles (Fig. 5, middle panel) reveal mainly negative meridional temperature gradients, as observed offshore, but they are marked by variations in their intensity due to the dynamics of the coastal ocean. However, due to coastal upwelling, the midshelf profile in summer (JAS) is quite different from the correspondent offshore profile. In summer, relative temperature

https://doi.org/10.5194/essd-2026-558
Preprint. Discussion started: 23 July 2026

Open Access Earth System Science Data Discussions

minima are located at the approximate latitudes of Cape Finisterre (CF), just south of river Minho (RM), Cape Carvoeiro (CC), and just south of Cape Roca (CR) and Cape Sines (CS). These locations are well correlated with the source areas of recurrently observed upwelling filaments that develop along the west Iberian coast (e.g., Fiúza 1983, Sousa and Bricaud 1992, Haynes et al. 1993). In summer, relative temperature maxima are located immediately to the north of RM and CC, between CC and CR, and between CR and CS. These temperature maxima are believed to be due to Ria's runoff buoyancy impact on shelf circulation (~ 42.5°N), and to the advection of warmer offshore waters into the shelf, either by upwelling recirculation mechanisms (~40ºN) or eddy circulation associated to major changes in coastline orientation (~38.5ºN) (see Relvas et al., 2007). At the northern limit of the midshelf line (the Galicia coast) the temperature meridional gradient clearly becomes positive northward of CF, reaching a relative maximum temperature of approximately 18ºC at 44ºN. This temperature pattern in northern Galicia is related to the break in the north-south orientation of the coast north of CF (see Fig. 1) - the coastline north of CF is not aligned with the predominant winds off Iberia in summer, which are northerly, and consequently there is little upwelling to reduce the local SST.

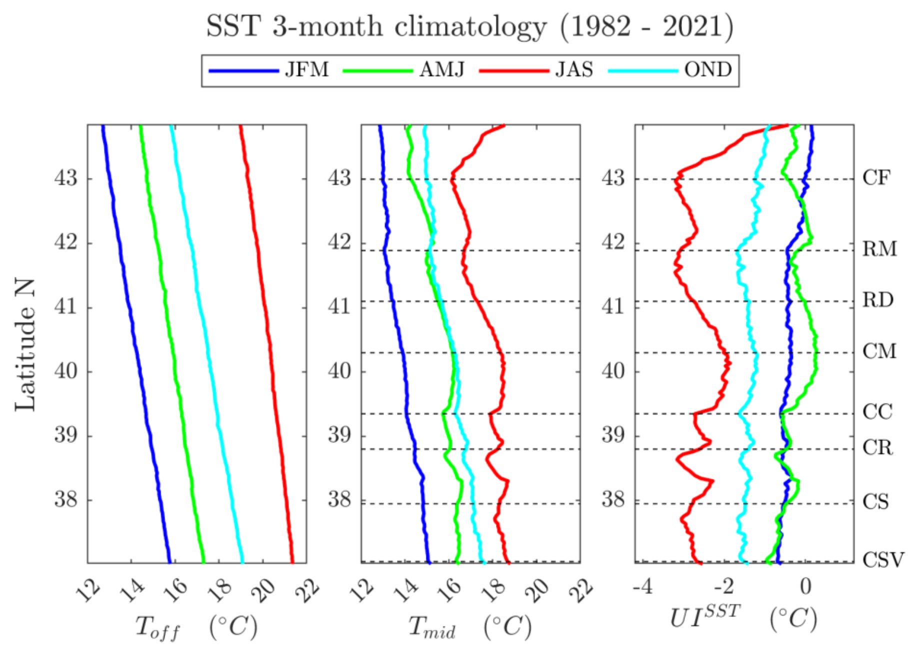

Figure 6. SST profiles for the 3-month climatology: (left panel) offshore SST, (middle panel) midshelf SST and (right panel) UI^{SST}.

https://doi.org/10.5194/essd-2026-558
Preprint. Discussion started: 23 July 2026

Since the upwelling index corresponds to the difference between the SST over the shelf and the SST offshore, the globally negative character of the meridional T^{off} and T^{mid} gradients disappear from the upwelling index profiles (Fig. 6, right panel). The latitudinal variability of the upwelling index profiles is clearly defined by the correspondent variability of T^{mid} profiles.

The upwelling index values approach zero from winter to spring, being positive in this last season in some parts of the west coast of the Iberian Peninsula. The most negative values of the upwelling index, corresponding to a larger intensity of the coastal upwelling, are obtained in the summer. In autumn, these values become slightly less negative, but its profile maintains the main characteristics of the summer profile. The sudden start of the upwelling season, when compared to its end, an aspect already identified in the weekly climatology, it is perfectly visible through the greater difference between the spring profile and the summer profile of the upwelling index, than between the latter and the autumn profile.

The SST variance for the 3-month climatology is shown in Fig. 7. The offshore SST variance (top row) shows a nearly homogeneous distribution with latitude, registering lower values during the winter season, as a consequence of the development of a well-stirred homogeneous, thick surface layer. During the other seasons there is a slight variance increase as we progress to autumn, with summer and autumn revealing a weak positive meridional variance gradient. The midshelf SST variance (Fig. 7, middle row) is globally at the same level of the correspondent 3-month variance at the offshore profiles, but shows, apart from the winter season, a clear latitudinal dependence. This is a consequence of a more complex wind-driven ocean dynamics over an almost meridional oriented continental shelf, due to the presence of the bottom at relatively shallow depths and a coastline acting as a lateral constraint to ocean flow. The midshelf variance is at all latitudes lowest in winter, again as a result of the development of a ticker mixed surface layer, and globally, as in the offshore case, there is a slight variance increase as we progress to autumn. As a direct consequence of the variability brought on by the surface signature of upwelled waters, summer's signal has a characteristic latitudinal structure that is still evident during autumn.

https://doi.org/10.5194/essd-2026-558
Preprint. Discussion started: 23 July 2026

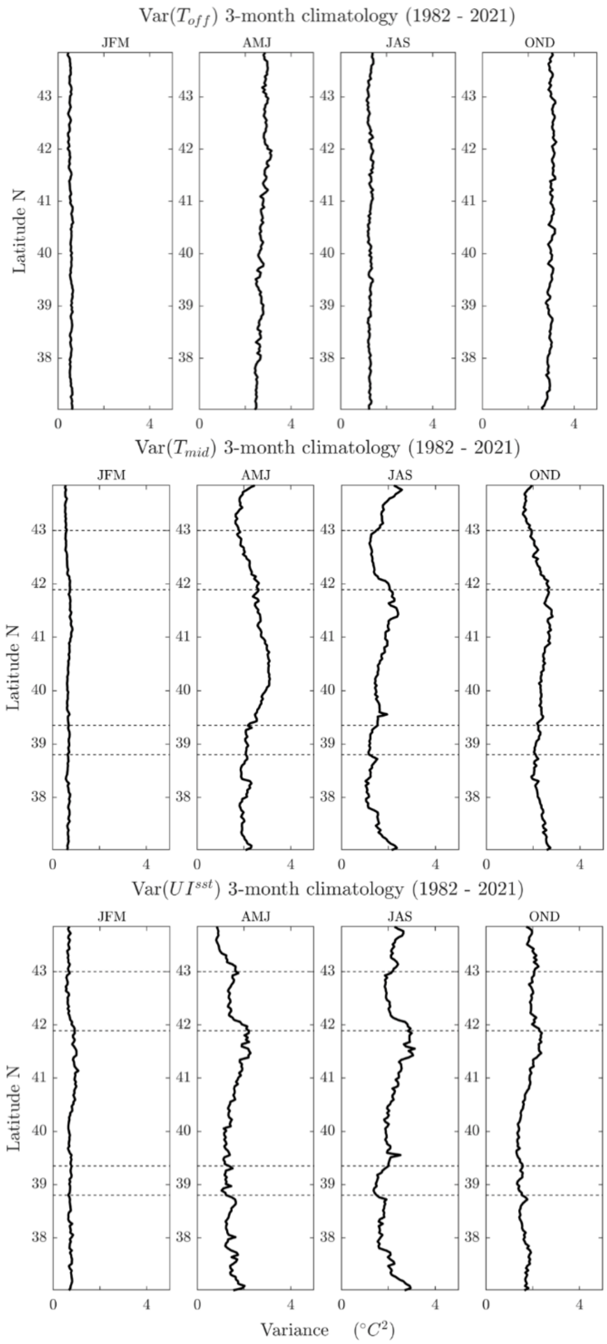

Figure 7. Meridional profiles of SST variance for the 3-month climatology: (top row) offshore SST; (middle row) midshelf SST; (bottom row) UI^{SST}. Panels from left to right are for winter (JFM), spring (AMJ), summer (JAS), and autumn (OND). The horizontal lines are drawn from north to south at the latitudes of CF, RM, CC, and CR (see Fig. 1).

https://doi.org/10.5194/essd-2026-558
Preprint. Discussion started: 23 July 2026

The maxima and minima of the midshelf summer SST variance revealed the time and geographical variability of the west Iberian upwelling. A maximum variance value is located in the 41º-42ºN latitudinal interval. This maximum is most probably associated to the irregular presence in space and time of an upwelling filament centered at a mean position of approximately 41.5ºN (Haynes et al., 1993). The intermittent character of this filament is linked to the dynamical nature of its formation. According to Haynes et al. (1993), this filament is caused by flow instabilities of the southward upwelling coastal jet, that may be instigate by the meandering effect produced on the current by the upstream large capes of Galicia.

Also noticeable, is a strong increasing trend of midshelf summer SST variability approaching the northern and the southern limits of the midshelf line, where a change in the orientation of the coast occurs, from the meridional western coast to the northern and southern zonal Iberian coasts. These higher values of SST variance should be justified by the interplay of the costal ocean dynamics of the western Iberian with the coastal dynamics of the Gulf of Biscay, on the north, and of the Gulf of Cadiz, on the south. In the southern limit, Relvas and Barton (2005, 2002) refer that at times of upwelling relaxation, there is an interaction of two contrasting regimes in the region: a southward advection flow of cold western coast upwelled waters and a coastal poleward counterflow of warm southern coast origin waters. This fact should contribute to the observed increase in the summer SST variability in the region.

Concerning the minima of the midshelf summer SST variance, the lowest values spread in the latitudinal band ~38.0º-38.5ºN, just north of cape Sines in a region with a week negative summer upwelling index (see Fig. 5). The inflection on the meridional orientation of the coastline and of the associated depth contours at the northern limit of this region produces an upwelling sheltered area characterized by a stable relative warm anomaly during summer (Relvas et al., 2007).

The coast of the Galicia Rías, from approximately 42ºN to 43ºN, it is another region of relative low values of midshelf summer SST variance. This is clearly linked to the persistent upwelling and associated filament of Cape Finisterre (~43ºN), as a combined result of local bottom topography (Haynes et al., 1993) and summer wind field dominant patterns (Torres et al., 2003).

https://doi.org/10.5194/essd-2026-558
Preprint. Discussion started: 23 July 2026

The variance of the upwelling index (Fig. 7, bottom row) is largely governed by midshelf SST variability, particularly in summer, when wind-driven coastal upwelling dominates the SST gradient between the coast and the adjacent open ocean.

4.2.3 Monthly climatology of the upwelling index

The monthly evolution of the UI^{sst} profile is shown in Fig. 8. From January to March, typical winter months for the ocean, UI^{sst} values tend to zero indicating no significant thermal contrast between the ocean surface at midshelf and the open ocean. Upwelling apparently starts in May near Cape Carvoeiro and Cape Roca and then in June near Cape Finisterre and Cape São Vicente. In July upwelling is well established south of Cape Carvoeiro and north of River Douro but only on the verge of starting in the region centered on Cape Mondego. The shape of the meridional profile of the upwelling index in July will remain until October, only the intensity of its values will vary. In August the UI^{sst} profile has sharpened and increased in amplitude, with strong upwelling centers now in evidence south of Cape Sines, near capes Roca and Carvoeiro and in the region between 42ºN and 43ºN. By September upwelling has reached its maximum amplitude all along the coast. The UI^{sst} profile starts weakening in October. Although the UI^{sst} profiles for November and December are still negative along the entire coast, it should not be thought that upwelling is still occurring. Upwelling can be said to have stopped when the spatial distribution of upwelling maxima and minima, as seen most clearly in the profiles from July to October, are no longer apparent. When the northerly winds cease, upwelled waters gradually ebb away as a result of shelf-deep ocean exchange and sea surface momentum and energy fluxes.

https://doi.org/10.5194/essd-2026-558
Preprint. Discussion started: 23 July 2026

Open Access Earth System Science Data Discussions

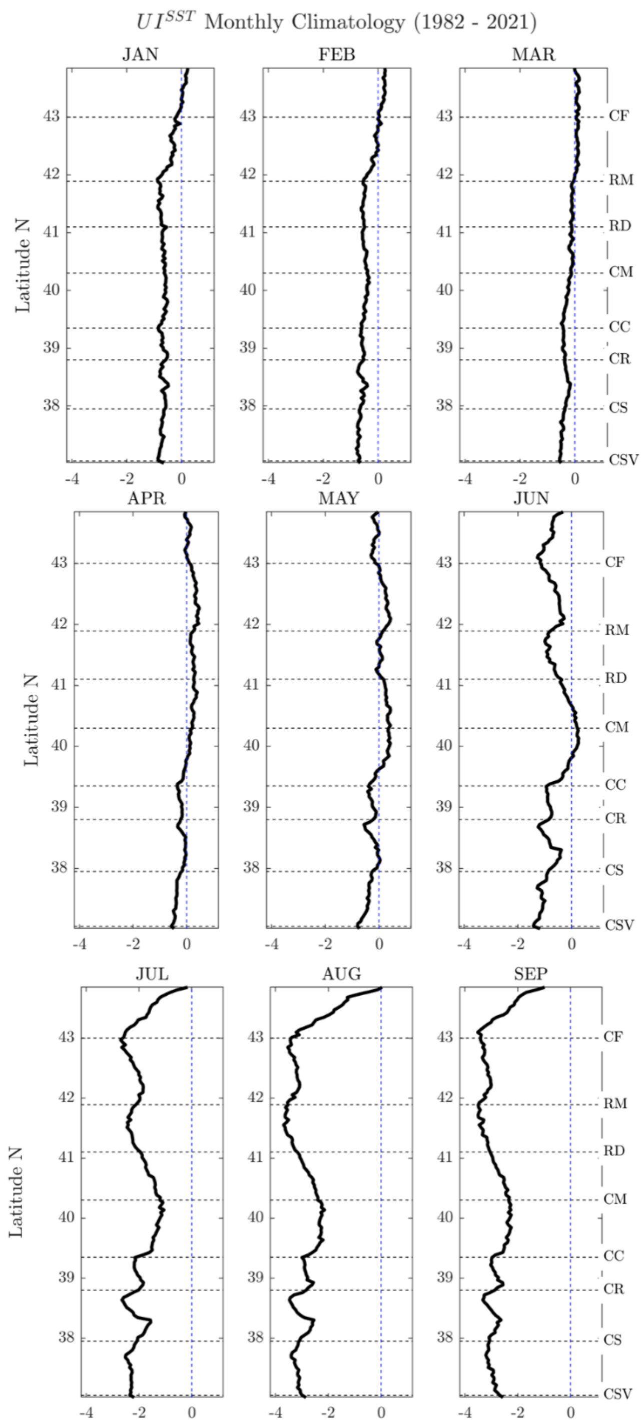

530 Figure 8. Monthly climatology of the upwelling index.

https://doi.org/10.5194/essd-2026-558
Preprint. Discussion started: 23 July 2026

In summary, the UI^{sst} monthly climatology depicted in Fig.8 shows that there is a lag in the starting time of the upwelling season between the region south (already visible in May/June) and north (evidence of a development in July) of Cape Carvoeiro. In both regions, it reaches its maximum intensity in September and ends in November.

5. Conclusions and Future Directions

The presence of clouds creates a large number of gaps in the sea surface temperature data derived from infrared satellite measurements. The number of gaps is increased further when differencing the data to calculate the SST upwelling index. The gaps can be eliminated by averaging, but at the expense of reduced space and time resolution, or, the missing data can be replaced using an interpolation methodology. Taking these aspects into account, the CoRTAD database was chosen, a 21-year global ocean SST satellite database, gap-free, with 4-km resolution and weekly-averaged. In this database, the problem of the absence of SST observations was tackled by using the night and day passes from the Pathfinder V5.3 satellite database and, by computing the weekly mean values. The gaps of SST values still present in the database were specifically filled using a 3x3 pixel median spatial fill and, if necessary, applying a piecewise cubic Hermite interpolating polynomial function. The obtained space and time resolution of the CoRTAD dataset is compatible with the observation of submesoscale to mesoscale coastal ocean processes.

From the CoRTAD database, SST values at near-coast and offshore locations were extracted and UI^{sst}, the coastal upwelling index was calculated. Near-coast and offshore locations vary according to local oceanographic and geographic characteristics of the study area. For West Iberia near-coast positions over the continental shelf between the shelf break and approximately 10 km from the coastline were used as the midshelf line, and a meridional line along 15 ºW as the offshore line. An upwelling index was obtained for West Iberia (37°-44°N) during the period 02 Jan 1982 — 31 Dec 2021.

Using the extracted SST dataset and the computed upwelling index, the midshelf climatology was investigated and found to accurately identify the spatial location of known recurrent upwelling centers along the coast of West Iberia. Previously these features had only been identified using individually selected cloud-free synoptic SST images (e.g., Fiúza, 1983; Sousa and Bricaud, 1992; Haynes et al., 1993) and are blurred or missing in climatological studies that average over space and time to get SST fields without missing data (e.g., Santos et al., 2005). Based on this result, we conclude that the upwelling index

https://doi.org/10.5194/essd-2026-558
Preprint. Discussion started: 23 July 2026

calculated from the CoRTAD dataset gives an accurate representation of the upwelling along West Iberia. The monthly climatology shows that there are no north-south differences in the upwelling intensity or the end of the upwelling season. However, it shows that the central region of the West Iberia, between Cape Carvoeiro (~39 ºN) and River Douro (~41 ºN), has a later start of the upwelling season, in July/August, when compared to the rest of the coast, in June/July.

Since 1999 there have been continuous measurements of ocean winds by satellite scatterometers. An Ekman upwelling index can be calculated using these winds and should be compared with the SST upwelling index.

Data availability

The West Iberia SST Upwelling Index dataset described in this paper is openly available through the CoastNet community on Zenodo at https://doi.org/10.5281/zenodo.21458306 (Castellanos et al., 2026). The repository provides the complete dataset together with the associated metadata and documentation required for its interpretation and reuse.

Author contributions

Joaquim Dias designed the research and developed the methodology; Greg King supervised the processing of the datasets and developed the methodology; and Paola Castellanos supervised the analysis and wrote the manuscript.

Competing interests

The authors declare that they have no conflict of interest.

Acknowledgements

The CoRTAD Version 6 SST data were provided by the US National Centers for Environmental Information. This project was supported in part by a grant from the NOAA Climate Data Record (CDR) Program for satellites and the NOAA Coral Reef Conservation Program.

This work benefited from the Infrastructure CoastNet (http://geoportal.coastnet.pt), funded by Foundation for Science and Technology (FCT) and the European Regional Development Fund (FEDER), through LISBOA2020 and ALENTEJO2020 regional operational programmes, in the framework of the National Roadmap of Research Infrastructures of strategic relevance (PINFRA/22128/2016).

This publication was also financed by the Fundação para a Ciência e a Tecnologia (FCT) through the project UID/04292/2025 (https://doi.org/10.54499/UID/04292/2025), awarded to MARE and through the project LA/P/0069/2020 (https://doi.org/10.54499/LA/P/0069/2020) granted to the Associate Laboratory ARNET.

References

Alvarez, I., Gomez-Gesteira, M., deCastro, M., Dias, J.M., 2008. Spatiotemporal evolution of upwelling regime along the western coast of the Iberian Peninsula. J. Geophys. Res. Ocean. 113. doi:10.1029/2008JC004744

Álvarez-Salgado, X.A., Labarta, U., Fernández-Reiriz, M.J., Figueiras, F.G., Rosón, G., Piedracoba, S., Filgueira, R., Cabanas, J.M., 2008. Renewal time and the impact of harmful algal blooms on the extensive mussel raft culture of the Iberian coastal upwelling system (SW Europe). Harmful Algae 7, 849–855. doi:10.1016/j.hal.2008.04.007

Alvera-Azcárate, A., Barth, A., Beckers, J.M., Weisberg, R.H., 2007. Multivariate reconstruction of missing data in sea surface temperature, chlorophyll, and wind satellite fields. J. Geophys. Res. Ocean. 112, 1–11. doi:10.1029/2006JC003660

Alvera-Azcárate, A., Barth, A., Rixen, M., Beckers, J.M., 2005. Reconstruction of incomplete oceanographic data sets using empirical orthogonal functions: Application to the Adriatic Sea surface temperature. Ocean Model. 9, 325–346. doi:10.1016/j.ocemod.2004.08.001

https://doi.org/10.5194/essd-2026-558
Preprint. Discussion started: 23 July 2026

Ambar, I., Dias, J., 2008. Remote sensing of coastal upwelling in the north-eastern Atlantic Ocean, in: Barale, V., Gade, M. (Eds.), Remote Sensing of the European Seas. Springer, pp. 141–152. doi:10.1007/978-1-4020-6772-3_11

Arístegui, J., Alvarez-Salgado, X.A., Barton, E.D., Figueiras, F.G., Hernández-León, S., Roy, C., Santos, A.M.P., 2006. Oceanography and fisheries of the Canary Current/Iberian Region of the Eastern North Atlantic, in: Robinson, A.R., Brink, K.H. (Eds.), The Sea, 14B. Harvard University Press, pp. 877–932.

Arístegui, J., Barton, E.D., Álvarez-Salgado, X.A., Santos, A.M.P., Figueiras, F.G., Kifani, S., Hernández-León, S., Mason, E., Machú, E., Demarcq, H., 2009. Sub-regional ecosystem variability in the Canary Current upwelling. Prog. Oceanogr. 83, 33–48. doi:10.1016/j.pocean.2009.07.031

Bakun, A., 1973. Coastal upwelling indices, west coast of North America, 1946–1971. NOAA Tech. Rep. NMFS SSFR-671 103. doi:NMFSSSRF-671

Barton, E.D., 1998. Eastern boundary of the north Atlantic: Northwest Africa and Iberia coastal segment, in: Robinson, A.R., Brink, K.H. (Eds.), The Sea, 11. John Wiley and Sons, pp. 633–657.

Beckers, J.M., Barth, A., Alvera-Azcárate, A., 2006. DINEOF reconstruction of clouded images including error maps. Application to the Sea-Surface Temperature around Corsican Island. Ocean Sci. 2, 183–199.

Beckers, J.M., Rixen, M., 2003. EOF Calculations and Data Filling from Incomplete Oceanographic Datasets*. J. Atmos. Ocean. Technol. 20, 1839–1856. doi:10.1175/1520-0426(2003)020<1839:ECADFF>2.0.CO;2

Benazzouz, A., Mordane, S., Orbi, A., Chagdali, M., Hilmi, K., Atillah, A., Lluís Pelegrí, J., Hervé, D., 2014. An improved coastal upwelling index from sea surface temperature using satellite-based approach - The case of the Canary Current upwelling system. Cont. Shelf Res. 81, 38–54. doi:10.1016/j.csr.2014.03.012

Bograd, S.J., Schroeder, I., Sarkar, N., Qiu, X., Sydeman, W.J., Schwing, F.B., 2009. Phenology of coastal upwelling in the California Current. Geophys. Res. Lett. 36, 1–5. doi:10.1029/2008GL035933

Bustos, D.F., Narváez, D.A., Dewitte, B., Oerder, V., Vidal, M., Tapia, F., 2024. Revisiting historical trends in the Eastern Boundary Upwelling Systems with a

https://doi.org/10.5194/essd-2026-558
Preprint. Discussion started: 23 July 2026

machine learning method. Front. Mar. Sci. 11:1446766. doi: 10.3389/fmars.2024.1446766

Castellanos, P., Dias, J., et al.: The CoastNet Upwelling Index: A 4-km weekly sea surface temperature-derived upwelling dataset for the Iberian Peninsula (Version 1.0) [Data set], Zenodo, https://doi.org/XX.XXXX/zenodo.XXXXXXX, 2026

Demarcq, H., 1998. Spatial and Temporal Dynamics of the Upwelling off Senegal and Mauritania: Local Change and Trend, in: Durand, M.-H., Cury, P., Mendelssohn, R., Roy, C., Bakun, A., Pauly, D. (Eds.), Global versus Local Changes in Upwelling Systems. pp. 149–166.

Demarcq, H., Faure, V., 2000. Coastal upwelling and associated retention indices derived from satellite SST. Application to Octopus vulgaris recruitment. Oceanol. Acta 23, 391–408. doi:10.1016/S0399-1784(00)01113-0

FAO, 2022. The State of World Fisheries and Aquaculture 2022. Towards Blue Transformation. Rome, FAO. https://doi.org/10.4060/cc0461en

Fiúza, A.F.G., 1983. Upwelling patterns off Portugal, in: Suess, E., Thiede, J. (Eds.), Coastal Upwelling: Its Sediment Record. Plenum Press, pp. 85–98.

Fiúza, A.F.G., Macedo, M.E., Guerreiro, M.R., 1982. Climatological space and time-variation of the Portuguese coastal upwelling. Oceanol. Acta 5, 31–40.

Frouin, R., Fiúza, A.F.G., Ambar, I., Boyd, T.J., 1990. Observations of a poleward surface current off the coasts of Portugal and Spain during winter. J. Geophys. Res. Ocean. 95, 679–691. doi:10.1029/JC095iC01p00679

Haynes, R., Barton, E.D., 1990. A poleward flow along the Atlantic coast of the Iberian peninsula. J. Geophys. Res. Ocean. 95, 11425–11441. doi:10.1029/JC095iC07p11425

Haynes, R., Barton, E.D., Pilling, I., 1993. Development, persistence, and variability of upwelling filaments off the Atlantic coast of the Iberian Peninsula. J. Geophys. Res. 98, 22681–22692. doi:10.1029/93JC02016

Kilpatrick, K. A., Podestá, G. P., Evans, R., 2001. Overview of the NOAA/NASA advanced very high resolution radiometer Pathfinder algorithm for sea surface temperature and associated matchup database. J. Geophys. Res., 106(C5), 9179–9197. doi:10.1029/1999JC000065Kravtsov, S.K., Dewar, W.K., Ghil, M., Berloff,

https://doi.org/10.5194/essd-2026-558
Preprint. Discussion started: 23 July 2026

P.S., Mcwilliams, J.C., 2008. North Atlantic climate variability in coupled models and data. Nonlinear Process. Geophys. 15, 13–24.

Kriebel, K.T., Gesell, G., Kästner, M., Mannstein, H., 2003. The cloud analysis tool APOLLO: Improvements and validations. Int. J. Remote Sens. 24, 2389–2408. doi:10.1080/01431160210163065

Leitão, F., Baptista, V., Vieira, V., Laginha Silva, P., Relvas, P., Alexandra Teodósio, M., 2019. A 60-Year Time Series Analyses of the Upwelling along the Portuguese Coast. Water, 11, 1285. https://doi.org/10.3390/w11061285

Lemos, R.T., Pires, H.O., 2004. The upwelling regime off the west Portuguese coast, 1941-2000. Int. J. Climatol. 24, 511–524. doi:10.1002/joc.1009

Lemos, R.T., Sansó, B., 2006. Spatio-temporal variability of ocean temperature in the Portugal Current System. J. Geophys. Res. Ocean. 111, 1–14. doi:10.1029/2005JC003051

Marshall, J., Kushnir, Y., Battisti, D., Chang, P., Czaja, A., Dickson, R., Hurrell, J., McCartney, M., Saravanan, R., Visbeck, M., 2001. North Atlantic climate variability: Phenomena, impacts and mechanisms. Int. J. Climatol. 21, 1863–1898. doi:10.1002/joc.693

McClain, E.P., Pichel, W.G., Walton, C.C., 1985. Comparative performance of AVHRR-based multichannel sea surface temperatures. J. Geophys. Res. 90, 11586–11601. doi:10.1029/JC080i014p11587

Nykjær, L., Van Camp, L., 1994. Seasonal and interannual variability of coastal upwelling along northwest Africa and Portugal from 1981 to 1991. J. Geophys. Res. 99, 14197. doi:10.1029/94JC00814

Pauly, D., Christensen, V., 1995. Primary production required to sustain global fisheries. Nature 374, 255–257. doi:10.1038/374255a0

Peliz, Á., Dubert, J., Santos, A.M.P., Oliveira, P.B., Le Cann, B., 2005. Winter upper ocean circulation in the Western Iberian Basin - Fronts, Eddies and Poleward Flows: an overview. Deep. Res. Part I 52, 621–646. doi:10.1016/j.dsr.2004.11.005

Peliz, Á., Fiuza, A.F.G., 1999. Temporal and spatial variability of CZCS-derived phytoplankton pigment concentrations off the western Iberian Peninsula. Int. J. Remote Sens. 20, 1363–1403. doi:10.1080/014311699212786

https://doi.org/10.5194/essd-2026-558
Preprint. Discussion started: 23 July 2026

Peliz, Á., Rosa, T.L., Santos, A.M.P., Pissarra, J.L., 2002. Fronts, jets, and counter-flows in the Western Iberian upwelling system. J. Mar. Syst. 35, 61–77. doi:10.1016/S0924-7963(02)00076-3

Relvas, P., Barton, E.D., 2005. A separated jet and coastal counterflow during upwelling relaxation off Cape São Vicente (Iberian Peninsula). Cont. Shelf Res. 25, 29–49. doi:10.1016/j.csr.2004.09.006

Relvas, P., Barton, E.D., 2002. Mesoscale patterns in the Cape São Vicente (Iberian Peninsula) upwelling region. J. Geophys. Res. 107, 1–23. doi:10.1029/2000JC000456

Relvas, P., Barton, E.D., Dubert, J., Oliveira, P.B., Peliz, Á., da Silva, J.C.B., Santos, A.M.P., 2007. Physical oceanography of the western Iberia ecosystem: Latest views and challenges. Prog. Oceanogr. 74, 149–173. doi:10.1016/j.pocean.2007.04.021

Reynolds, R.W., Rayner, N.A., Smith, T.M., Stokes, D.C., Wang, W.Q., 2002. An improved in situ and satellite SST analysis for climate. J. Climate, 15, 1609–1625. doi: 10.1175/1520-0442(2002)015<1609:AIISAS>2.0.CO;2

Saha, K., Zhao, X., Zhang, H., Casey, K.S., Zhang, D., Zhang, Y., Baker-Yeboah, S., Relph, J.M., Krishnan, A., Ryan, T., 2018a. The Coral Reef Temperature Anomaly Database (CoRTAD) Version 6 - Global, 4 km Sea Surface Temperature and Related Thermal Stress Metrics for 1982 to 2019. Used subset: CoRTAD version 6_filled SST. NOAA National Centers for Environmental Information. Dataset. https://doi.org/10.25921/ffw7-cs39. Data accessed on June 2022.

Saha, K, Zhao, X., Zhang, H., Casey, K.S., Zhang, D, Baker-Yeboah, S., Kilpatrick, K.A., Evans, R.H., Ryan, T., Relph, J.M., 2018b. AVHRR Pathfinder version 5.3 level 3 collated (L3C) global 4km sea surface temperature for 1981-Present. NOAA National Centers for Environmental Information. Dataset. https://doi.org/10.7289/v52j68xx.

Sánchez, R.F., Relvas, P., Delgado, M., 2007. Coupled ocean wind and sea surface temperature patterns off the western Iberian Peninsula. J. Mar. Syst. 68, 103–127. doi:10.1016/j.jmarsys.2006.11.003

https://doi.org/10.5194/essd-2026-558
Preprint. Discussion started: 23 July 2026

Santos, A.M.P., Kazmin, A.S., Peliz, Á., 2005. Decadal changes in the Canary upwelling system as revealed by satellite observations: Their impact on productivity. J. Mar. Res. 63, 359–379. doi:10.1357/0022240053693671

Santos, A.M.P., Peliz, Á., Dubert, J., Oliveira, P.B., Angélico, M.M., Ré, P., 2004. Impact of a winter upwelling event on the distribution and transport of sardine (Sardina pilchardus) eggs and larvae off western Iberia: a retention mechanism. Cont. Shelf Res. 24, 149–165. doi:10.1016/j.csr.2003.10.004

Selig, E.R., Casey, K.S., Bruno, J.F., 2010, New insights into global patterns of ocean temperature anomalies: implications for coral reef health and management. Global Ecology and Biogeography, 19: 397-411. https://doi.org/10.1111/j.1466-8238.2009.00522.x

Siemer, J.P., Machín, F., González-Vega, A., Arrieta, J. M., Gutiérrez-Guerra, M. A., Pérez-Hernández, M. D., Vélez-Belchí, P., Hernández-Guerra, A., Fraile-Nuez, E., 2021. Recent trends in SST, Chl-a, productivity and wind stress in upwelling and open ocean areas in the upper Eastern North Atlantic subtropical gyre. Journal of Geophysical Research: Oceans, 126, e2021JC017268. doi:10.1029/2021JC017268

Sousa, F.M., Bricaud, A., 1992. Satellite-derived phytoplankton pigment structures in the Portuguese upwelling area. J. Geophys. Res. 97, 11343–11356. doi:10.1029/92JC00786

Torres, R., Barton, E.D., Miller, P., Fanjul, E., 2003. Spatial patterns of wind and sea surface temperature in the Galician upwelling region. J. Geophys. Res. 108, 1–14. doi:10.1029/2002JC001361